RADIAL AND NONRADIAL OSCILLATION MODES IN RAPIDLY ROTATING STARS

C. C. LOVEKIN AND R. G. DEUPREE
Institute for Computational Astrophysics, Department of Astronomy and Physics, Saint Mary's University, Halifax, NS B3H 3C3, Canada;
clovekin@ap.smu.ca

ABSTRACT

We use two-dimensional stellar models and a two-dimensional finite difference integration of the linearized pulsation equations to calculate nonradial oscillations. This approach allows us to directly calculate the pulsation modes for a distorted rotating star without treating the rotation as a perturbation. We are also able to express the finite difference solution in the horizontal direction as a sum of multiple spherical harmonics for any given mode. Using these methods, we have investigated the effects of increasing rotation and the number of spherical harmonics on the calculated eigenfrequencies and eigenfunctions and compared the results to perturbation theory. We use 10 $M_\odot$ models with velocities ranging from 0 to 420 km s^{-1} ($0.89\Omega_c$) and examine low-order p-modes. We find that one spherical harmonic remains reasonable up to a rotation rate around 300 km s^{-1} ($0.69\Omega_c$) for the radial fundamental mode, but can fail at rotation rates as low as 90 km s^{-1} ($0.23\Omega_c$) for the $l = 2$ p_2 mode, based on the eigenfrequencies alone. Depending on the mode in question, a single spherical harmonic may fail at lower rotation rates if the shape of the eigenfunction is taken into consideration. Perturbation theory, in contrast, remains valid up to relatively high rotation rates for most modes. We find the lowest failure surface equatorial velocity is 120 km s^{-1} ($0.30\Omega_c$) for the $l = 2$ p_2 mode, but failure velocities between 240 and 300 km s^{-1} ($0.58\Omega_c$–$0.69\Omega_c$) are more typical.

Subject headings: stars: oscillations — stars: rotation

1. INTRODUCTION

Stellar oscillations provide us with a probe of the internal structure of stars. The oscillations depend on the stellar structure and are modified by factors such as rotation, magnetic fields, and tidal forces. In theory, if we have sufficiently accurate parameters for a star, we can produce models which will constrain the internal structure. Unfortunately, due to the uncertainties on the temperature and luminosity of the star and the large number of free parameters (mass, rotation rate, age, etc.), this process is much more difficult in practice. Accurate modeling also requires enough observed modes to actually place some constraints on the star. The more modes available, the tighter these constraints can be, but we must be sure that all the modes used are real. Artificial or extraneous modes can make it impossible to produce a matching model. In recent years, the number of stars with multiple modes has increased greatly, thanks to both the ground-based networks such as STEPHI (Belmonte et al. 1993) and WET (Nather et al. 1990) as well as space-based observations such as *WIRE* (Hacking et al. 1999) and *MOST* (Walker et al. 2003). Current and upcoming space missions, such as *Kepler* (Basri et al. 2005) and *COROT* (Baglin et al. 2001), are expected to further increase the number of multiperiodic variables. Unfortunately, the theory still lags behind the observations, particularly for rotating stars.

The first investigation of nonradial oscillations was undertaken by Pekeris (1938). This paper derived the linearized, adiabatic equations for nonradial oscillations of nonrotating stars, and then solved the equations for models of uniform density. At the time, it was assumed that nonradial modes would be subject to significant amounts of damping, more so than the purely radial modes. As a result, nonradial oscillations were generally not studied extensively. However, these assumptions do not hold for the low-order p-modes or for all g-modes. Unlike radial oscillations, which are unstable only for $\gamma < \frac{4}{3}$, there are some nonradial oscillations of a uniform density sphere which are unstable for all values of γ. Based on these results, Pekeris (1938) concluded that nonradial

oscillations must be considered. Using these results, Cowling (1941) calculated the periods of nonradial oscillations for nonrotating polytropes.

Before the advent of numerical techniques, these equations had to be solved using analytical methods. Much of this work was done by Chandrasekhar, who explored the variational principle as a method of solving the linear adiabatic pulsation equations (Chandrasekhar & Lebovitz 1962; Chandrasekhar 1964). This method depends on an arbitrary guess at the form of the eigenfunction, and the resulting eigenvalues depend on the guess. Fortunately, even marginal guesses at the eigenfunction can produce reasonable results for the eigenfrequencies with this method. This approach is largely unused today, as it has been superseded by computational work using more efficient and accurate numerical techniques.

The first direct numerical integration of the linearized equations for nonradial oscillations was performed by Hurley et al. (1966). In this work, they calculated oscillation frequencies for nonrotating, polytropic stellar models, for comparison with the earlier analytic approaches discussed above. Although they restricted themselves to polytropic models, their method can relatively easily be extended to more realistic stellar models.

All of these approaches depend on perturbations to a nonrotating (i.e., spherical) stellar model. In this case, the calculations are relatively straightforward. Rotation, even moderate rotation, can significantly complicate the calculation, and many attempts have been made over the years to solve the problem with varying degrees of success. These will be discussed in more detail below.

In spherical stars, the solution to the linear adiabatic pulsation equations is separable and can be written as

$$\xi_r = X(r)Y_l^m(\theta, \phi). \tag{1}$$

The angular variation can be characterized by a single spherical harmonic, Y_l^m, and both l and m are legitimate quantum

numbers. Once a star becomes distorted, e.g., through tidal effects or rotation, the situation becomes more complex and several problems arise. The eigenfunction can no longer strictly be described by a single spherical harmonic, and thus l is no longer a valid quantum number. As long as the star remains axisymmetric, m remains valid. As well as changes in the structure of the eigenfunction, the pulsation frequencies themselves will change. It is this change in eigenfrequency that has been of most interest to researchers, particularly as observations continue to find more and more rotating and pulsating stars, many with multiple frequencies.

One of the earlier attempts to solve the linear adiabatic pulsation equations for rotating stars was made by Chandrasekhar & Lebovitz (1962), who applied the virial theorem to rotating incompressible fluids. The variational principle has also been extended to include slowly rotating stars by Clement (1964, 1965). Further attempts at improving the method through a better choice of basis vectors have also been made by Clement (1986). Although the variational equations themselves can be applied to a star with an arbitrary rotation rate (Ω), the method also depends on being able to model the structure of the star. The structure of rotating stars has generally been modeled as a perturbation to the nonrotating structure. Because the structural perturbations are limited to modeling slowly rotating stars, the variational method was also limited to slowly rotating stars.

An approach used more frequently now is based on a perturbation approach, as developed by Saio (1981). In this framework, the rotation is treated as a perturbation on the structure of the star. For example, the radial location in a rotating model would be written as

$$r = a[1 + \epsilon(a, \theta, \phi)]. \tag{2}$$

The linearized pulsation equations are expanded in a series in powers of the rotation rate. The zeroth power merely gives the nonrotating eigenvalues and eigenfunctions. Each nonrotating eigenfunction can be written in terms of a single spherical harmonic, and the eigenfunction can be characterized by three quantum numbers, one relating to the number of radial nodes and the two angular quantum numbers, l and m, associated with the spherical harmonics. The first order in the expansion in powers of the rotation rate lifts the $2l + 1$ fold degeneracy in the eigenvalues, while the eigenfunctions that correspond to this order are still characterized by a single spherical harmonic.

We note that this will not be true in the general set of linearized pulsation equations of a rotating star. The coefficients of the perturbations in the pulsation equations, composed of terms based on the static rotating model, will have latitudinal variations. The eigenfunctions will also have a latitudinal variation, so that the equations can be expressed as products of spherical harmonics, which in turn can be written as sums of spherical harmonics through appropriate recursion relations.

In perturbation theory the rotation rate is assumed to be much smaller than the frequency being calculated. This keeps the rotational perturbation "small" so that including only the first one or two terms in the power series expansion is satisfactory. "Small" is, of course, a vague term, and it is not clear how small is "small." Based on discussions at the Workshop on the Future of Asteroseismology held in Vienna in 2006 September, estimates of the limiting rotation rate ranged from 50 to 300 km s^{-1}. Of course, the limiting surface equatorial velocity will be dependent on the mass of the star in question.

Efforts to more accurately include rotation have been developed. These methods require two-dimensional (2D) calculations,

so they are more time-consuming and complex. As a result, previous studies have all faced restrictions and limitations. For example, Espinosa et al. (2004) calculated the adiabatic oscillations of rapidly rotating stars with uniform rotation. To succeed, they applied the Cowling approximation, neglected the Coriolis force, and neglected the Brunt-Väisälä frequency in the adiabatic equation. Yoshida & Eriguchi (2001) have modeled quasi-radial modes at a range of rotation rates in rotating neutron stars using the relativistic Cowling approximation. Other methods, such as that employed by Lignières et al. (2006) and Reese et al. (2006), have fewer physical restrictions, but have so far been restricted to explorations of polytropic models.

The effects discussed in this paper are only expected to matter for stars undergoing moderate to rapid rotation. A recent study of OB stars (Daflon 2007) found that 50% of OB stars have rotation velocities greater than 100 km s^{-1}. At least some of these stars are expected to pulsate. For example, β Cephei–type pulsations have been detected in Spica (Sterken et al. 1986), which is also rotating with a $v \sin i \sim 160$ km s^{-1}. For the β Cephei stars as a category, the projected rotation velocities range from 0 to 300 km s^{-1} (Stankov & Handler 2005). The average $v \sin i \sim 100$ km s^{-1}, although this could be a selection effect, as the highest amplitude pulsators are the more slowly rotating stars. Another category of pulsating stars, the low-amplitude δ Scuti (LADS) stars, have been detected with $v \sin i$ up to 250–300 km s^{-1} (Breger 2007). The models we consider in this paper are 10 $M_\odot$ zero-age main sequence (ZAMS) models with solar ($Z = 0.02$) metallicity. Although β Cephei stars have evolved along the main sequence, the trends produced by these models should be comparable to typical β Cephei stars. One effect which may be important is mode bumping, which will appear in real β Cephei stars but does not appear in our unevolved models. Our models include uniform rotation at rates from 0 to $0.89\Omega_c$. Our method also allows us to consider differential rotation, which will be discussed in a future paper.

Clement (1998) has developed a finite difference method for directly evaluating the eigenfunctions on a 2D grid. In this paper, we combine this method with 2D stellar models produced by ROTORC (Deupree 1990, 1995). The combination of these two approaches bypasses many of the restrictions faced by previous approaches. Our numerical methods and models are described in more detail in § 2. We investigate the effects of rotation on the calculated eigenfrequencies (§ 3) and eigenfunctions (§ 4), with the aim of establishing the range of validity of modes calculated with one spherical harmonic. In § 5 we compare our results with those predicted by second-order perturbation theory.

2. METHOD

Our stellar models are calculated using the 2D stellar evolution code ROTORC (Deupree 1990, 1995), allowing us to self-consistently model the surface and structure of the star for rotation rates from zero up to near-critical rotation. In this paper we focus on uniformly rotating 10 $M_\odot$ ZAMS models with $X = 0.7$, $Z = 0.02$. We use the OPAL opacities (Iglesias & Rogers 1996) and equation of state (Rogers et al. 1996) in these calculations. These models are fully 2D, with 10 angular zones from pole to equator and 349 radial zones. We have computed a few models using 20 angular zones and find differences in the horizontal variation of the density to be only about 0.1%. The pulsation code uses Fourier transform interpolation to convert from our angular zoning to its own angular zoning, and we feel the ROTORC angular zoning is not a major source of error in the calculations and use our 10 angular zone models in this work.

The location of the surface of the stellar model is found by assuming it lies on an equipotential surface. The value of the equipotential is determined by the value of the total potential in the angular zone which has the largest radius (for uniformly rotating models, this is always at the equator). The radial zone which has this value of the total potential is found at each angular zone and the surface boundary conditions applied there. One source of inaccuracy is that a radial zone is either completely interior or completely exterior to the surface, so that the surface is defined as the radial zone interface which is closest to the location of the equipotential. Our rotating models are made by imposing a surface equatorial velocity and an internal angular momentum distribution (in this case, uniform rotation) and allowing the surface to change as needed. This can lead to small differences between the imposed (target) surface equatorial velocity and the actual surface equatorial velocity, typically less than 2 km s^{-1}. Throughout this paper, we refer to models by the target surface equatorial velocity.

For our pulsation calculations, we use the nonradial oscillation code (NRO) developed by Clement (1998). Instead of expressing the solution as a sum of spherical harmonics, the code solves the perturbation equations on a 2D spherical grid. In ROTORC, the stellar model is defined on a spherical polar grid, with the stellar surface location being an equipotential surface as discussed above. NRO transforms this into a model defined on surfaces of constant density. The 2D nature of the code allows us to account for the effect of the centrifugal distortion, but the Coriolis force is neglected. The pressure perturbation can be expressed in two ways:

$$\delta P(r, \theta, \phi; l, m, n) = e^{im\phi} \sum_{l=m}^{\infty} a_l^m(r; n, l) P_l^m(\cos\theta)$$

or

$$= e^{im\phi} \sum_{k=m}^{\infty} A_k^m(r, \theta; n, l) r^k.$$

In this code, the second form of this general equation is used. Keeping this general solution in mind, the linear adiabatic pulsation equations can be recast using five variables, related to the radial and angular velocity perturbation, the pressure and gravity perturbations, and the radial derivative of the gravitational perturbation. These variables are defined as follows:

$$y_1 \equiv \frac{\xi_r}{r^{k-1} \sin^m\theta},$$
$$y_2 \equiv \frac{\xi_\theta}{r^{k-1} \sin^{m-1}\theta \cos\theta},$$
$$y_3 \equiv \frac{\delta p}{r^k \sin^m\theta},$$
$$y_4 \equiv \frac{\delta\phi}{r^k \sin^m\theta},$$
$$y_5 \equiv \partial_r y_4, \tag{3}$$

where k is the radial exponent, m is the azimuthal quantum number, and $k = 0$ and $m = 0$ are special cases. If $k - 1$ and $m - 1$ are negative, they are replaced by 1. This form of the equations allows the boundary conditions to be applied while avoiding singularities. With these variables, the relevant linearized equations can be expressed in the general form:

$$\partial_r y_i = f(y_i, \partial_r y_{j\neq i}, \partial_\theta y_i). \tag{4}$$

The full form of the equations and their derivations can be found in Clement (1998).

The coefficients of the finite difference expressions of the equations (as represented in eq. [4]) covering the entire 2D grid can be put in a band diagonal matrix. Each element of this band diagonal matrix is itself a matrix, containing the coefficients at each zone in the 2D grid. The solution of the finite difference pulsation equations proceeds in two steps, from the center outward and from the surface inward. Each integration also requires an initial guess of the eigenfrequency.

The inward and outward integrations of the eigenfunctions are required to be continuous at some intermediate fitting surface. Once all of the coefficients of the equations have been evaluated, a subset of the matrix, including the fitting surface and the radial zones immediately surrounding it, can be inverted to solve for the perturbations at the fitting surface and the radial zone either directly above or directly below the fitting surface. These values can then be used to step inward and outward through the mesh to solve for the perturbations throughout the rest of the grid. At some point on the surface, one of the perturbations is forced to be a constant (typically, $\delta r/r = 1$) to eliminate the trivial solution of all variables being zero everywhere. As a result, there is one condition that has not been used. This can be used to evaluate a discriminant, which will only be satisfied (equal to zero) if an eigenvalue has been located. Using this method, we can step through eigenfrequency space, solving the matrix, evaluating the discriminant, and looking for zero crossings. Once a crossing has been located, various convergence schemes can be used to calculate the exact eigenfrequency. This method can miss frequencies when two eigenfrequencies are quite close together, although these can usually be avoided by reducing the frequency step size.

The code can include up to nine angular zones in the solution for the eigenfunctions, performing one radial integration for each angle included. At the end of the calculation, the solution is known at N angles, which can subsequently be decomposed into the contributions of individual spherical harmonics. This is done with Fourier transforms, which transform the N discrete points into coefficients of the appropriate cosine series. After some algebraic manipulation, this series is converted into a Legendre series, which gives us the relative contribution of each Y_l^m (or Legendre polynomial for the case in which $m = 0$). Because each radial integration contains angular derivatives, also evaluated using finite differencing, the resultant coupling among spherical harmonics arises naturally. Thus, this method allows us to directly model the coupling among spherical harmonics in a single pulsation mode for rotating stars in a natural way.

Because l is not a legitimate quantum number for rotating models, specifying l is not necessary. In the pulsation code the input value of l is used to specify the parity of the mode, not the exact value of l. Based on the parity of l, the code includes the first k even or odd basis functions, where k is the input value of the number of angular zones to be included. We limit ourselves to small input values of l because those are expected to be the most easily observable. We also restrict ourselves to axisymmetric modes ($m = 0$), although this is not a constraint intrinsic to the method. We have also restricted ourselves to modes with small radial quantum number (n).

Because l is no longer a valid quantum number, we need a new designation for mode identification. We have chosen to identify the mode with a quantum number, l_0, which is the value of l of the mode in the nonrotating model to which a given mode can be traced back. This tracing back is based on examining both the eigenfrequency and the angular shape of the eigenfunction (the modes at different radial quantum numbers are easy to resolve;

no mode bumping is exhibited in these ZAMS models). This is quite easy up to moderate rotation rates because one spherical harmonic tends to dominate. This method fails for rotation velocities above 420 km s^{-1} because no spherical harmonic dominates. For rotation velocities above 360 km s^{-1}, we find this method becomes somewhat uncertain and produces an irregular progression in frequency for some modes. We thus consider the pulsation properties for models up to 420 km s^{-1}, but regard the frequencies above 360 km s^{-1} as uncertain. Although we only consider pulsation up to 420 km s^{-1}, our static models go up to near-critical rotation.

3. ACCURACY OF EIGENFREQUENCIES

As described in the above section, NRO, combined with 2D structure models from ROTORC, allows us to calculate the eigenfrequencies for a rotating star without making any a priori assumptions about the structure of the star. The method of solution of NRO allows for the inclusion of multiple spherical harmonics. As a result, we can calculate eigenfunctions for distorted stars including the coupling between spherical harmonics. In contrast most current calculations and observations generally assume that pulsation frequencies and observed modes can be characterized by a single spherical harmonic. It is therefore of interest to determine at what surface equatorial velocity modes can no longer be adequately described by a single spherical harmonic.

One of the issues arising out of the following discussion is where a difference between two calculated modes becomes significant. Both ground-based and space-based observations continue to improve, as new projects are continuously launched (figuratively and literally). As an example, *COROT* is expected to measure frequencies to a precision of less than 0.01 μHz for the long runs, and better than 0.065 μHz for a faint object during short runs (Michel et al. 2007). Based on these numbers, calculated frequencies do not need to change by much to be outside the observational uncertainties. However, we must ask ourselves whether it is reasonable to expect our models to match this accuracy. The linear adiabatic pulsation code uses 10^{-6} as the convergence criterion on the discriminant described in § 2. There will be other sources of error on the final eigenfrequency, such as from the finite difference representation of the pulsation equations. Neglecting these other sources of error, NRO converges modes to an accuracy of about 10^{-6}, or about 0.001 μHz, more than sufficient to match the predicted *COROT* accuracy. However, there are inaccuracies that result from the finite difference zoning in the static models. When we change the surface equatorial velocity from one model to the next, we change the distribution of material in the star, although the radial zoning (fractional surface equatorial radius) remains the same. The changes become larger as the rotation rate increases. This is equivalent to changing the radial zoning, for which experience from the early calculations of linear radial pulsation indicated a sensitivity on about the 1% level. We have also fairly dramatically rezoned a couple of our models and found that the eigenfrequencies changed on about the 1% level, or about 8.5 μHz for our models. The higher radial order p-modes are slightly more affected because the outer layers of the model, where the gradients of model quantities are steeper, play a larger role. Clearly, our ability to measure observational frequencies to high precision is irrelevant until models improve enough to match them. Until then, for changes induced by rotational effects to be considered significant, they must be larger than our model uncertainties.
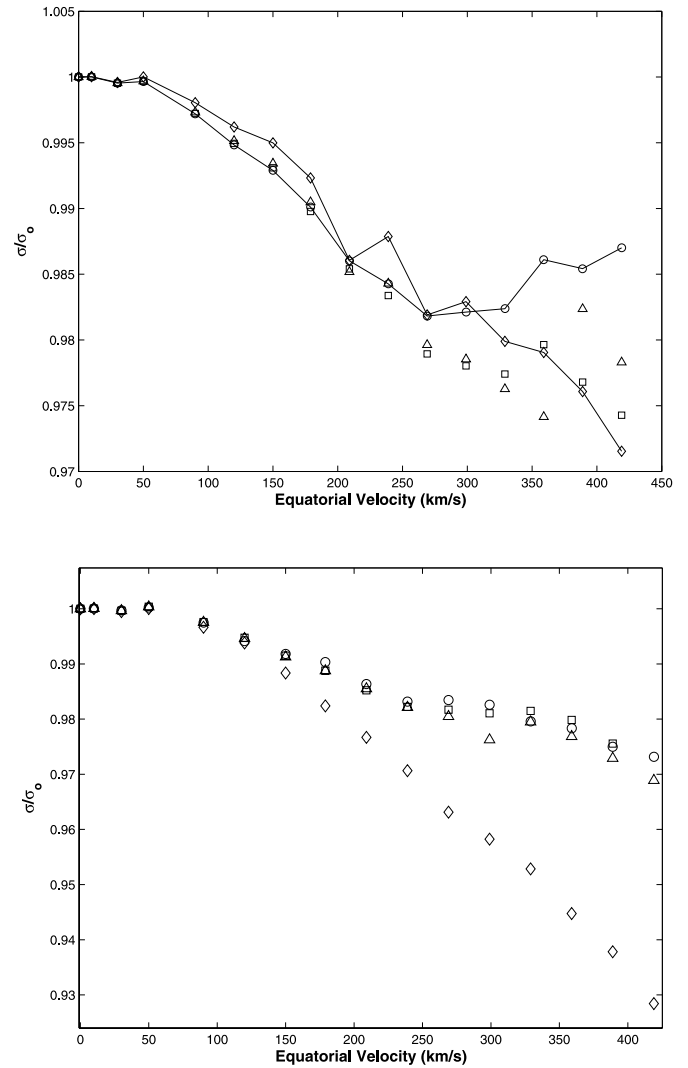

Fig. 1.—Frequency changes as a function of surface equatorial velocity for the fundamental mode for $l_0 = 0$ (*top*) and $l_0 = 1$ (*bottom*). Frequencies shown are calculated with one Y_l^m (*diamonds*), two Y_l^m's (*circles*), three Y_l^m's (*squares*), and six Y_l^m's (*triangles*).

Another uncertainty consideration is the angular resolution of our pulsation calculations. As described above, the number of spherical harmonics used in NRO determines the number of radial integrations performed. There are several ways we can assess the effects of this changing angular resolution. First, we would expect the slowly rotating modes to be relatively unaffected by angular resolution. This is indeed what we find. In the case of slow rotation, the coefficients for the higher order spherical harmonics are small, typically not more than a percent up to 120 km s^{-1}. Over these same rotation ranges, we also expect the frequency to be relatively unaffected by angular resolution, and this is indeed what we find. The frequencies shown in Figure 1 differ by less than a quarter of a percent over this rotation range.

In the majority of our plots, we show our results as a function of surface equatorial velocity, as this is the unit most easily compared to observations. However, for comparison with other models, it is more useful to show results as a function of angular rotation rate expressed as a fraction of critical rotation (Ω/Ω_c). Critical rotation was calculated using a model rotating at 575 km s^{-1}, with an equatorial radius of 5.792 $R_\odot$. This model is quite close to critical rotation. We have summarized the conversion between

TABLE 1
SUMMARY OF MODEL PARAMETERS

Target v_{eq} (km s^{-1})	Actual v_{eq}	Ω (10^{-3} s^{-1})	Ω/Ω_c	R_{eq} ($R_\odot$)	R_p/R_{eq}	T_p/T_{eq}
0..................	0	0.0000	0.00	3.973	1.000	1.000
10..................	9.97	0.0036	0.03	3.973	1.000	1.000
30..................	29.91	0.0108	0.08	3.976	0.999	1.001
50..................	49.85	0.0180	0.13	3.981	0.997	1.003
90..................	89.72	0.0322	0.23	4.000	0.991	1.008
120..................	119.63	0.0428	0.30	4.021	0.986	1.013
150..................	149.54	0.0531	0.37	4.048	0.977	1.021
180..................	179.45	0.0632	0.44	4.082	0.967	1.032
210..................	209.35	0.0729	0.51	4.125	0.953	1.051
240..................	239.26	0.0824	0.58	4.175	0.924	1.065
270..................	269.17	0.0913	0.64	4.237	0.908	1.082
300..................	299.08	0.0998	0.69	4.307	0.887	1.100
330..................	328.98	0.1076	0.76	4.393	0.866	1.125
360..................	358.89	0.1148	0.81	4.491	0.846	1.149
390..................	388.80	0.1215	0.85	4.600	0.821	1.173
420..................	418.71	0.1272	0.89	4.729	0.796	1.203

TABLE 2
SUMMARY OF VELOCITIES AT WHICH ONE Y_l^m FAILS
TO ACCURATELY REPRODUCE THE MODE

l_0 (1)	n (2)	Frequency[a] (3)	$\mathcal{D}\nu$[b] (4)	Eigenfunction[c] (5)
0..................	0	>360	. . .	165
	1	240	160	60
	2	180	24	25
1..................	0	210	. . .	110
	1	210	140	105
	2	180	30	85
2..................	0	. . .	. . .	75
	1	. . .	. . .	60
	2	. . .	. . .	45
3..................	0	. . .	. . .	70
	1	. . .	. . .	85
	2	. . .	. . .	. . .

[a] Limiting surface equatorial velocity based on frequency differences larger than 1%.
[b] Limiting surface equatorial velocity based on difference in the large separation greater than 1 μHz.
[c] Limiting surface equatorial velocity based on eigenfunctions with mean differences larger than 0.06.

these two frames of reference, as well as some other parameters of our models, in Table 1.

3.1. *Frequency Changes*

The simplest way to determine where the assumption that a single Y_l^m can be used is to compare the frequencies as calculated with different numbers of spherical harmonics. This is illustrated in Figure 1, which shows the normalized frequencies for the $l_0 = 0$ and 1 fundamental modes, as calculated using 1, 2, 3, and 6 spherical harmonics. At some cutoff surface equatorial velocity, the eigenfunctions calculated with only a few spherical harmonics begin to deviate significantly from those calculated using six spherical harmonics. For the $l_0 = 0$ mode, the frequencies calculated with one spherical harmonic are in reasonably good agreement to quite high velocities, remaining within approximately 0.5% of the frequencies calculated with more spherical harmonics. The $l_0 = 1$ mode as calculated with one spherical harmonic rapidly diverges from the frequencies as calculated with multiple basis functions. In this case, the single spherical harmonic frequency reaches a difference of 1% at a surface equatorial velocity of 210 km s^{-1} ($0.51\Omega_c$).

Similar results are found for higher order modes. These results are summarized in Table 2. To determine the location of the cutoff surface equatorial velocity, as described above, we take a difference of 1% to be significant, as discussed in § 3.

Although the periods are expected to change depending on the details of the model, period differences are expected to be much more stable. Hence, in the next subsection, we will consider the large separation and period ratios of our frequency calculations.

3.2. *Large Separations*

We have studied the large separation between the $n = 0$, 1, and 2 modes for $l_0 = 0$–3. We have calculated the large separations in the usual way:

$$\Delta\nu = \nu_{l,n+1} - \nu_{l,n}. \tag{5}$$

Before comparing these for the effects of the number of spherical harmonics included, we need to account for rotation, which

can change the large separation by changing the model structure. First, we normalize these large separations with respect to the nonrotating model:

$$D\nu = \Delta\nu(v = 0) - \Delta\nu(v). \tag{6}$$

We can then use these normalized large separations to look for the effects of the number of spherical harmonics included in the calculation (N):

$$\mathcal{D}\nu = D\nu_N - D\nu_{N=6}. \tag{7}$$

For this calculation, we have assumed that the frequencies calculated with six Y_l^m's are closest to the true pulsation frequencies, so the smaller the differences between this and other calculations, the more accurate the smaller number of spherical harmonics. This is illustrated in Figure 2, which shows the results of equation (7) as a function of surface equatorial velocity for the separation between the $l_0 = 0$ fundamental and first harmonic.

The uncertainty in the theoretical calculations of large separation is inversely proportional to the uncertainty in the radius of the stellar model in question. Taking the uncertainty in radius to be the size of one radial zone, for our models, this is approximately 0.04 μHz. Observationally, large separations are well determined for solar-type stars, with uncertainties typically less than 1 μHz. As a conservative estimate, we have chosen 1 μHz as our significance criterion, as shown by the dashed lines in Figure 2. It should be noted that once the large separations with one and two spherical harmonics begin to diverge, they do so quite rapidly, so unless the cutoff criterion is appreciably smaller ($\lesssim 0.5$ μHz), the cutoff surface equatorial velocity is not an extremely sensitive function of the cutoff criterion. The limiting rotational velocities estimated using the large separations are summarized in column (4) of Table 2.

4. ACCURACY OF EIGENFUNCTIONS

So far, the limiting rotation rates entered in Table 2 have been for the $l_0 = 0$ and 1 modes only. This is a result of the way
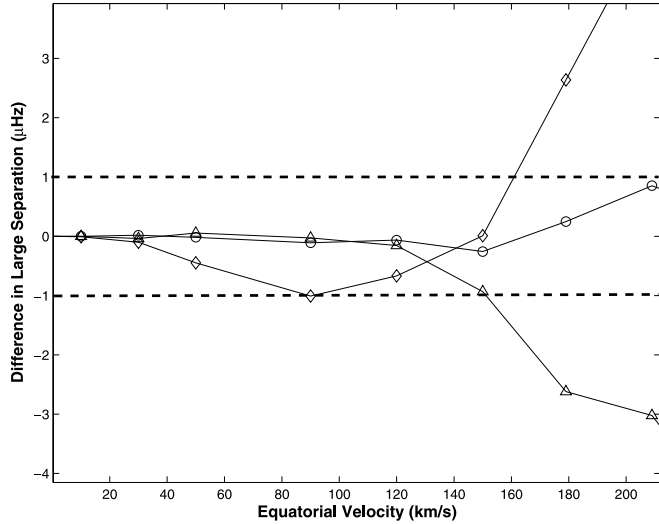
Fig. 2.—Relative large separation (eq. [7]) as a function of surface equatorial velocity between the $l_0 = 0$ fundamental and first harmonic, for one spherical harmonic (*diamonds*), two spherical harmonics (*triangles*), and three spherical harmonics (*circles*), all relative to six spherical harmonics. Dashed lines indicate the significance criterion adopted in this work.

spherical harmonics are included in NRO. To calculate the $l_0 = 2$ mode, for example, the code will select even Y_l^m starting with $l_0 = 0$, so at least two Y_l^m's are required. This is true for any mode with $l_0 \geq 2$. As a result, we cannot directly compare eigenfrequencies calculated with several spherical harmonics to those calculated with a single spherical harmonic.

We can still compare the eigenfunctions, and in this section this is what we will do. One of the advantages of including several spherical harmonics is the ability to study the effect of rotation not only on the eigenfrequencies, but also on the shapes of the eigenfunctions. For a nonrotating object, regardless of how many spherical harmonics are included, the eigenfunction remains a pure Y_l^m, as it should. As the rotation rate increases, neighboring spherical harmonics begin to contribute progressively more to the shape of the eigenfunction. These effects could be quite important for mode identification and need to be considered in rapidly rotating stars. One technique for mode identification uses the pulsation amplitudes in different colors as determined by single spherical harmonics. With rotation significantly altering the modes by coupling spherical harmonics, it could alter these color amplitudes and change the mode identification. We find that the effects of the coupling can become significant, even at very moderate rotation rates.

We have used a combination of the value of the eigenfrequency and the angular variation of the eigenfunction at the surface to identify the modes as we progressed from one rotating model to the next. Of course, with the finite difference approach the angular variation of the eigenfunction can vary with depth. Figure 3 presents this variation for several rotation rates for the $l_0 = 2$ fundamental mode. Each plot contains the variation at several different depths. As expected, the variation with depth is small for slowly rotating models and grows as the rotation rate increases. Despite this growth in variation, the profile remains recognizably the same until the most rapid rotation rate presented. This occurs at a rotation rate at which we are already beginning to have trouble tracing the modes from one rotation rate to the next, as we have previously mentioned.

Figure 4 shows the angular variation at the surface in the radial component of the $l_0 = 0$ fundamental mode at 90 and 270 km s^{-1}. At 90 km s^{-1}, the distorting effects of rotation are

negligible, although the differences are visible. In contrast, by 270 km s^{-1} the differences between the numbers of spherical harmonics are quite significant, and one spherical harmonic is clearly not sufficient to model the horizontal shape of the mode. In comparison, the *eigenfrequencies* were considered to be accurate using one spherical harmonic up to rotation rates of 300 km s^{-1}. This highlights the truism that even marginal eigenfunctions can give reasonable eigenfrequencies. By 270 km s^{-1}, the mode no longer looks like an $l = 0$ mode, nor even an $l = 2$, but is beginning to distinctly show the characteristics of the $l = 4$ contribution. These two velocities were chosen based on the relative contribution of each Y_l^m, shown for the radial fundamental mode in Figure 5. At 90 km s^{-1}, with all three sets of basis functions, the $l = 0$ component contributes nearly 100%, while at 270 km s^{-1}, the contribution of the same component drops below 50% when six spherical harmonics are considered.

From Figure 5, we can see that with two and three spherical harmonics, all of the spherical harmonics contribute a relatively significant amount by the time the model is rotating at intermediate speeds. In contrast, with six spherical harmonics, the contribution from the highest order spherical harmonics ($l = 10$) remains small out to at least 300 km s^{-1}. Although the contribution starts to become significant at very high rotation rates ($v \gtrsim 350$ km s^{-1}), it still remains a factor of 2–3 lower than the main contributors. From this, we have taken the shape of the eigenfunction with six spherical harmonics as being the most correct and have used it as a basis of comparison.

Based on the results shown in Figure 4, we know that one spherical harmonic ceases to be sufficient somewhere between 90 and 270 km s^{-1}. From Figure 5, we can see that the relative contribution of the Y_0^m drops below 90% at a surface equatorial velocity between 150 and 180 km s^{-1}. The angular variations of the eigenfunctions for these two velocities are shown in Figure 6. It is at this point that we would say multiple spherical harmonics are required to accurately reproduce the shape of the mode (see Figure 6).

We have developed a quantitative measure of how the shapes of the eigenfunction differ from that calculated using six spherical harmonics. This estimate is calculated by taking the absolute value of the difference between the six-basis function eigenfunction (standard) and one of the other eigenfunctions (comparison) at nine points. These points are equally spaced across the surface of the model, with $\theta = 10i$. The point at $\theta = 0$ is excluded, as all the eigenfunctions are normalized to 1 at this point. These differences are then squared and summed. The square root of the sum is normalized by the number of points to give a measure of how different the two curves are:

$$\text{mean difference} = \frac{1}{n}\sqrt{\sum_{i=1}^{n}(a_i - b_i)^2}. \qquad (8)$$

This difference as a function of surface equatorial velocity is shown in Figure 7. The differences between the eigenfunctions calculated with one, two, and three spherical harmonics relative to six spherical harmonics rise sharply starting at a surface equatorial velocity of 180 km s^{-1}. Based on this rise and the eigenfunctions shown in Figure 6, we estimate that when the mean difference rises above 0.06, more spherical harmonics are needed to accurately reproduce the shape of the mode.

For the other modes, the results are qualitatively similar, although the extent of the differences varies. The results for all four l_0 values considered in this paper are summarized in Table 2. Overall, one spherical harmonic remains a good approximation
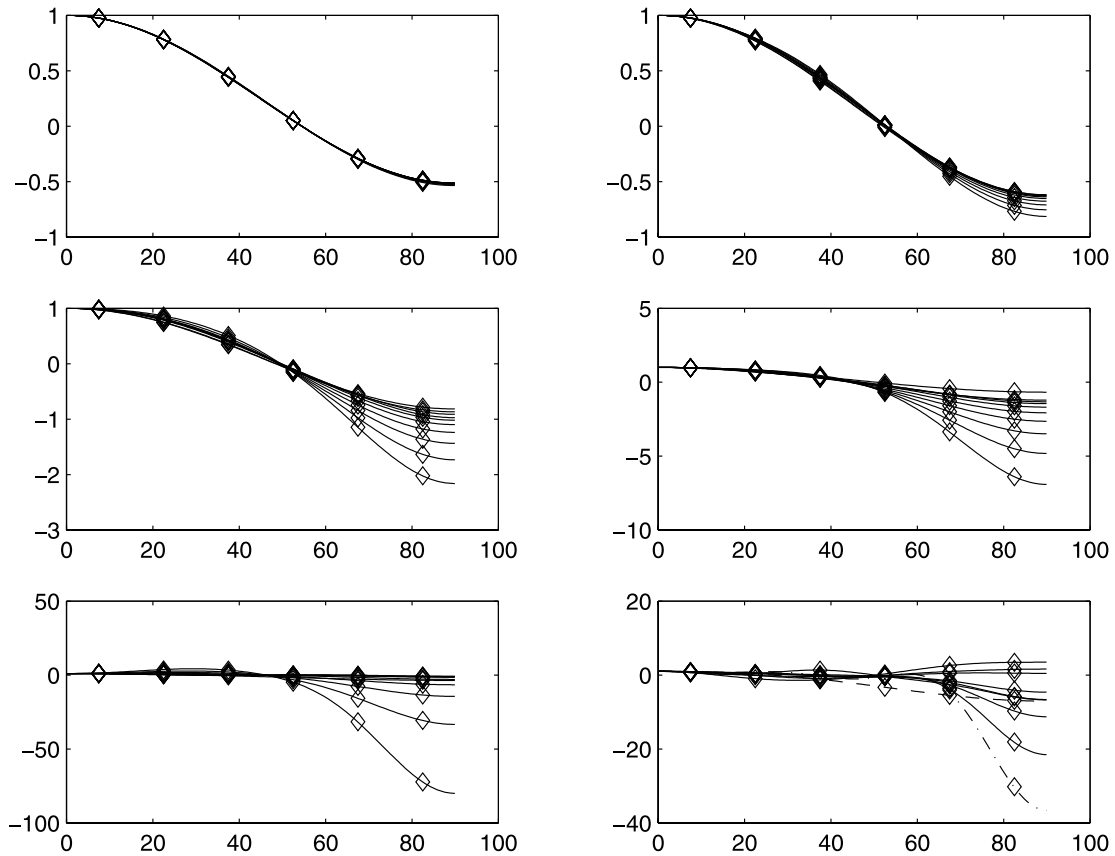
FIG. 3.— Variation in the radial eigenfunction for the $l_0 = 2$ mode as a function of colatitude at various depths (fractional surface equatorial radii of approximately 0.1, 0.2, 0.3, 0.4, 0.5, 0.6, 0.7, 0.8, 0.9, and 1.0) for models rotating at 50 km s^{-1} (*top left*), 150 km s^{-1} (*top right*), 240 km s^{-1} (*middle left*), 300 km s^{-1} (*middle right*), 360 km s^{-1} (*bottom left*), and 420 km s^{-1} (*bottom right*). The convective boundary is located between $0.2R_{eq}$ and $0.3R_{eq}$. The variation at each depth is normalized to be unity at the pole for purposes of comparison. The variation is smallest at the center of the star, and increases toward the surface. On the plot for 420 km s^{-1} (*bottom right*), the layer closest to the center is indicated with a dashed line, and the layer closest to the surface is indicated by a dot-dashed line. In most cases, 420 km s^{-1} is the most rapidly rotating model considered, as mode identification becomes difficult.
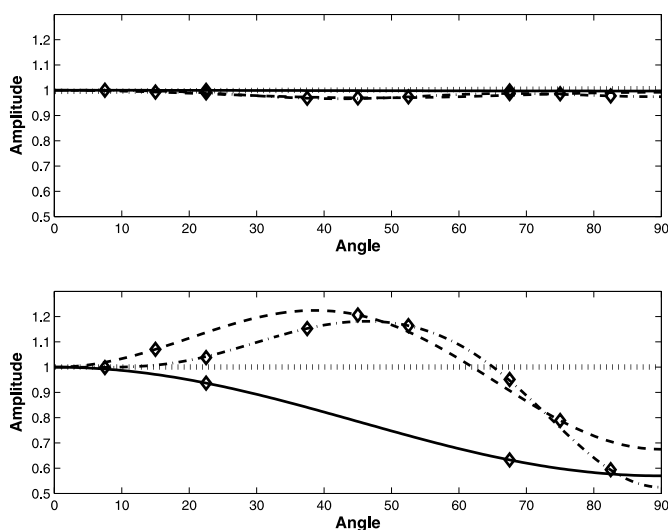
FIG. 4.—Angular variation in the radial eigenfunction for the radial fundamental mode of a model rotating at 90 km s^{-1} (*top*) and 270 km s^{-1} (*bottom*). On both plots, the shape of the eigenfunction is shown as calculated using one (*dotted line*), two (*solid line*), three (*dashed line*), and six (*dot-dashed line*) spherical harmonics.
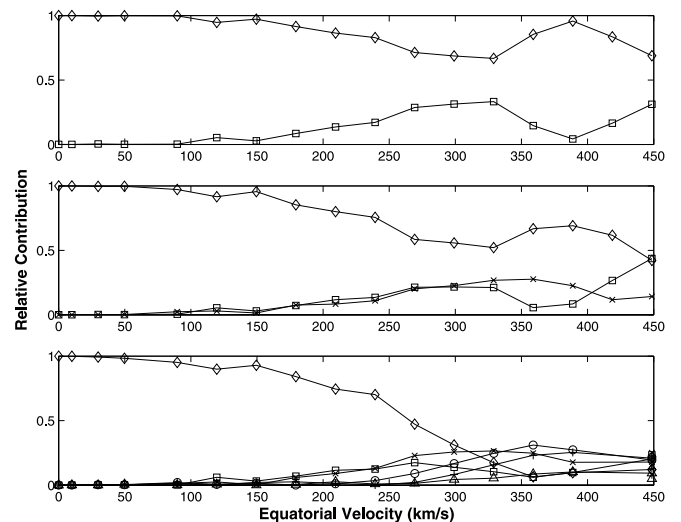

FIG. 5.—Relative contribution to the *f*-mode of each spherical harmonic for two (*top*), three (*middle*), and six (*bottom*) spherical harmonics, for $l = 0$ (*diamonds*), $l = 2$ (*squares*), $l = 4$ (*crosses*), $l = 6$ (*circles*), $l = 8$ (*plus signs*), and $l = 10$ (*triangles*). In the top plot, after $v \sim 150$ km s^{-1}, the contribution from $l_0 = 0$ drops below $\sim 90\%$ and we say that you need more spherical harmonics to be able to model the mode.
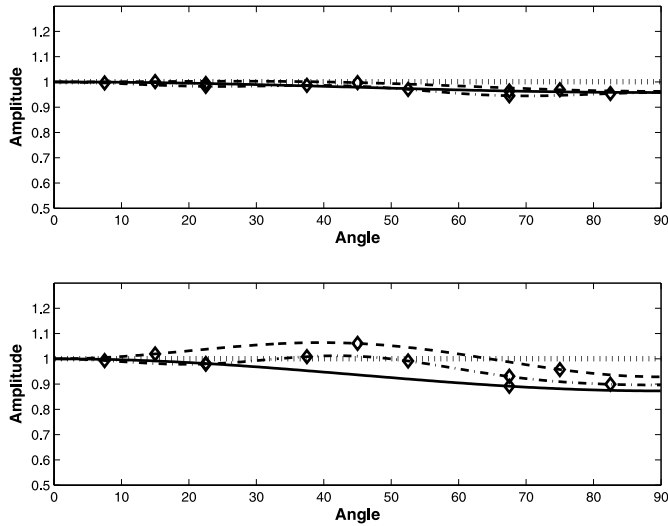
FIG. 6.—Same as Fig. 4, but for the velocities on either side of the cutoff surface equatorial velocity. At the lower velocity (150 km s^{-1}, *top*), the shape can be calculated reasonably well using one Y_l^m, but at the higher velocity (180 km s^{-1}, *bottom*), two or more are needed to accurately reproduce the horizontal variation in the eigenfunction.

FIG. 7.—Mean difference between the shape of the radial fundamental eigenfunction with six spherical harmonics and a pure P_0 mode (*diamonds*), two spherical harmonics (*squares*), and three spherical harmonics (*triangles*). Although there is some variation, all three curves show a sharp rise beyond 200 km s^{-1}. See text for the definition of the mean difference.

out to at least 90 km s^{-1} ($0.23\Omega_c$). For some modes, such as the radial fundamental, this approximation remains valid to much higher rotation rates (270 km s^{-1}, $0.64\Omega_c$). As both the angular and radial order of the mode increase, the limiting surface equatorial velocity decreases. In most cases, we find that the differences among calculations with different numbers of spherical harmonics grow quickly as a function of surface equatorial velocity once the differences become sizeable. We can conclude that our results are not particularly sensitive to the exact value of the cutoff criterion we have chosen, as long as it is not significantly lower than what we have used. We also find that comparing frequencies or frequency differences produces approximately the same results. Based on our results for a 10 $M_\odot$ model, a single spherical harmonic is never a good approximation for rotation rates above $0.64\Omega_c$, appears to always be a good approximation for rotation rates below $0.23\Omega_c$, and must be used with caution for rotation rates between these two values. Although there may be some mass effects, we do not expect these results to change significantly for masses close to 10 $M_\odot$.

5. COMPARISON WITH PERTURBATION THEORY

Second-order perturbation theory is routinely used to compute linear pulsation modes for rotating stars in which the centrifugal forces are expected to affect the pulsation frequencies. It has been difficult to comment on when second-order perturbation theory can be expected to fail because there have been few calculations of eigenfrequencies using other methods. Our approach will allow placing some limits on the range of applicability of second-order perturbation theory, but again these limits will be a product of the accuracy obtainable or required.

Second-order perturbation theory shows that, for such axisymmetric modes as we consider here, the change in eigenfrequency is a linear function of the square of the rotation rate (e.g., Saio 1981). We shall compare our results with this linear relation in two separate ways, both of which determine the failure of perturbation theory by a deviation from this linear relation. Of course, the result will depend on the quantitative value as to when the deviation becomes significant, a point we will discuss at the end of this section. We shall use the results we feel most accurately
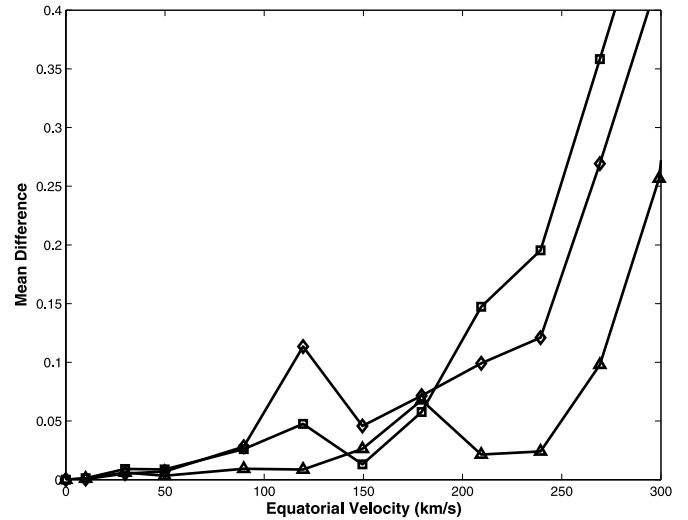
reflect the true values of the pulsation frequencies, the results with six angular zones in the 2D pulsation grid, for our comparison of eigenfrequencies.

The first method starts with the first four models in the rotation sequence (surface equatorial rotation velocities from 0 to 90 km s^{-1}). We calculate the best fit to the linear relationship, as given by perturbation theory, and the standard deviation. We repeat this exercise, each time adding one more model to the analysis, until all rotation velocities are included. As long as the linear relation is satisfied, we expect the standard deviation to be approximately constant as we add results for more rapidly rotating models. At some point, as the rotation becomes more rapid, the standard deviation will become larger and at some threshold value will be declared no longer to be an adequate representation of a straight line. Thus, second-order perturbation theory would no longer be considered reliable. We plot this standard deviation as a function of the rotation rate of the most rapidly rotating member of each sample in Figure 8. We somewhat arbitrarily set our threshold at 4×10^{-6} as being a value above the flat region for all modes. The values for the limits of applicability of perturbation theory computed by this method are listed in column (3) of Table 3. We have also examined the slope of each linear fit and, as expected, find that the slope changes gradually where the linear fit is good, and more rapidly as more points are added.

One difficulty with the above approach is that the coefficients of the linear fit change as more rapidly rotating models are added. A more constraining determination of the threshold of perturbation theory might be obtained by using the first few members of the sequence to determine the coefficient of the linear fit. The assumption is that the slope that perturbation theory would predict is correctly computed using the first few slowly rotating members of the sequence. We use the first five members in our rotation sequence to calculate this coefficient. We then use this coefficient to determine perturbation theory frequencies at each of our surface equatorial velocities. As before, we take the differences between the two methods as significant when they are larger than 1%. The results for this method are listed in column (4) of Table 3. We compare our pulsation frequencies with those predicted assuming the coefficient computed for the first four
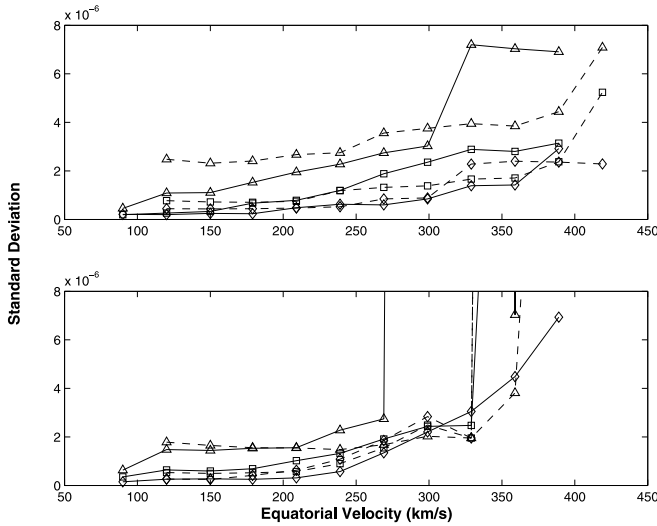
FIG. 8.—Standard deviation from a straight line as more points are included for the $l_0 = 0$ and 1 modes (*top*) and $l_0 = 2$ and 3 modes (*bottom*), for fundamental mode (*diamonds*), first harmonic (*squares*), and second harmonic (*triangles*). We take the cutoff standard deviation to be 4×10^{-6}. Solid lines represent the even modes (0, 2), and dashed lines represent the odd modes (1, 3).

members of the sequence is valid at all rotational velocities in Figure 9.

We find the trends for both methods of evaluating the threshold are similar for the two methods, but that the thresholds computed for the coefficient fit are more constrained. This is to be expected because forcing a linear fit to have a certain slope is more confining than merely forcing a fit to be linear. It is interesting that the threshold for perturbation theory occurs at generally higher rotation speeds than the threshold for the validity of a single spherical harmonic. The extrapolation of the linear fit to higher rotation velocities is flatter than our calculation with six angular zones and much flatter than our calculation with only one angular zone.

Our results indicate that perturbation theory is satisfactory to appreciably larger rotation velocities than the results of Reese et al. (2006), who found that third-order perturbation theory failed for rotation rates above about $0.2\Omega_c$. Much of this difference arises from the much tighter constraint they placed on what dif-
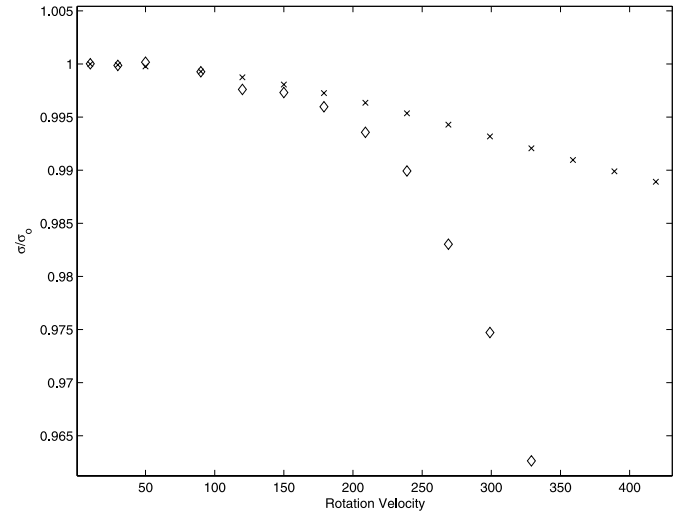
TABLE 3
SUMMARY OF VELOCITIES AT WHICH PERTURBATION THEORY FAILS
TO ACCURATELY REPRODUCE THE MODE

l_0 (1)	n (2)	Linear Fit (3)	Coefficient Fit (4)	One Y_l^{m}[a] (max/min) (5)
0......................	0	...	360	>360/160
	1	...	240	240/60
	2	300	270	180/25
1......................	0	...	...	210/110
	1	>360	330	210/105
	2	360	210	180/30
2......................	0	330	240	75
	1	330	180	60
	2	270	120	45
3......................	0	330	210	70
	1	330	210	85
	2	360	330	...

[a] Maximum and minimum rotation speeds at which one Y_l^m is valid, where more than one criterion exists.

FIG. 9.—Normalized frequencies as calculated with NRO (*diamonds*) and using an estimate of the perturbation theory results (*crosses*) for the $l_0 = 2$ *f*-mode.

ference in eigenvalues is significant. They are able to do this because they perform their comparisons using polytropes, which can be numerically integrated very accurately, whereas we use finite difference techniques to generate our more realistic stellar models. A subsidiary consideration is that they can control both the total mass and radius, and thus can arbitrarily scale from one model to the next, whereas our models include the conservation of energy, which removes the radius as an arbitrary parameter. In addition, the surface locations at each angle of our rotating models are quantized; the surface is regarded to include the full radial zone instead of fractions of zones. Our errors are in line with variations in eigenvalues computed for radial modes at a similar stage of development (e.g., Castor 1971). We believe these errors are reasonable at the present time because the deduced properties of the stars observed will be inaccurate both from the conversion from observed parameters to theoretical parameters and from the uncertainties in the effects of inclination on the relation between the observed and intrinsic properties. The model and parameter inaccuracies will be far greater than the error in the observed frequencies. Physical uncertainties, particularly in the internal angular momentum distribution, are expected to be greater than or equal to the uncertainties in an individual model, particularly for the more rapidly rotating stars in which we are interested ($v > 200$ km s^{-1}). We believe that being able to compute the evolution of the rotation law as the star ages may, at this stage, play a more important role than increasing the accuracy of the calculations. Of course, we recognize that improvements in accuracy on all fronts are valuable.

6. CONCLUSIONS

In this paper, we have attempted to test the validity of two independent assumptions commonly made in calculating stellar oscillation frequencies. These are first that the nonradial modes can be modeled using a single Y_l^m, and second that the modes can be calculated using second-order perturbation theory out to some limiting (highly uncertain) rotation rate.

We find that when a single spherical harmonic becomes inaccurate is mode dependent, with it failing at lower rotation velocities for higher order modes. The answer is also different depending on what property one examines. A single spherical harmonic is sufficient to reproduce frequencies to within 1% for rotation velocities up to at least 180 km s^{-1} ($0.44\Omega_c$), and for some low-order modes may even be valid up to 390 km s^{-1} ($0.85\Omega_c$). In

contrast, the angular shapes of the eigenfunctions are extremely sensitive to rotation, and the assumption fails at a maximum surface equatorial velocity of 165 km s^{-1}. In most cases, the assumption fails at much lower rotation velocities, typically around 50–75 km s^{-1}. Period differences (large separations) are expected to be of most interest, and these are also found to be sensitive to the order of the mode. A single spherical harmonic can accurately predict the difference between the fundamental and first harmonic of the $l_0 = 0$ and 1 mode up to velocities of around 150 km s^{-1} ($0.37\Omega_c$). The higher order modes are very sensitive to rotation, and the assumption fails at velocities around 25–30 km s^{-1} ($0.08\Omega_c$). One interesting consequence of the limitations of a single spherical harmonic is the impact it may have on mode identification, which is most often based on comparing the variation in pulsation amplitude with color, with models computed assuming a single spherical harmonic (e.g., Heynderickx et al. 1994).

We have compared our eigenfrequencies with the relation between eigenfrequency and rotation rate predicted by second-order perturbation theory. The relationship is followed reasonably well for models rotating up to surface rotational velocities of about 400 km s^{-1} for very low order modes. The relation fails at lower rotational velocities (approximately 200 km s^{-1} or $\Omega/\Omega_c = 0.58$) for modes with two or three radial nodes. These values are dependent on the difference between the two sets of frequencies tolerated. In these calculations, the limits are determined by the properties of the rotating stellar models rather than the calculations of the eigenfunctions.

REFERENCES

Baglin, A., et al. 2001, in Proc. SOHO 10/GONG 2000 Workshop, ed. A. Wilson (ESA SP-464; Noordwijk: ESA), 395
Basri, G., Borucki, W. J., & Koch, D. 2005, NewA Rev., 49, 478
Belmonte, J. A., et al. 1993, in IAU Colloq. 137, Inside the Stars, ed. W. W. Weiss & A. Baglin (ASP Conf. Ser. 40; San Francisco: ASP), 739
Breger, M. 2007, Commun. Astroseismology, 150, 25
Castor, J. I. 1971, ApJ, 166, 109
Chandrasekhar, S. 1964, ApJ, 139, 664
Chandrasekhar, S., & Lebovitz, N. R. 1962, ApJ, 135, 248
Clement, M. J. 1964, ApJ, 140, 1045
———. 1965, ApJ, 141, 210
———. 1986, ApJ, 301, 185
———. 1998, ApJS, 116, 57
Cowling, T. G. 1941, MNRAS, 101, 367
Daflon, S., Cunha, K., de Araújo, F. X., Wolff, S., & Przybilla, N. 2007, AJ, 134, 1570
Deupree, R. G. 1990, ApJ, 357, 175
———. 1995, ApJ, 439, 357
Espinosa, F., Pérez Hernández, F., & Roca Cortés, T. 2004, in Proc. SOHO 14/GONG 2004 Workshop, ed. D. Danesy (ESA SP-559; Noordwijk: ESA), 424

Hacking, P., et al. 1999, in ASP Conf. Ser. 177, Astrophysics with Infrared Surveys, ed. M. D. Bicay, R. M. Cutri, & B. F. Madore (San Francisco: ASP), 409
Heynderickx, D., Waelkens, C., & Smeyers, P. 1994, A&AS, 105, 447
Hurley, M., Roberts, P. H., & Wright, K. 1966, ApJ, 143, 535
Iglesias, C. A., & Rogers, F. J. 1996, ApJ, 464, 943
Lignières, F., Rieutord, M., & Reese, D. 2006, A&A, 455, 607
Michel, E., Baglin, A., Samadi, R., Baudin, F., & Auvergne, M. 2007, Commun. Astroseismology, 150, 341
Nather, R. E., Winget, D. E., Clemens, J. C., Hansen, C. J., & Hine, B. P. 1990, ApJ, 361, 309
Pekeris, C. L. 1938, ApJ, 88, 189
Reese, D., Lignières, F., & Rieutord, M. 2006, A&A, 455, 621
Rogers, F. J., Swenson, F. J., & Iglesias, C. A. 1996, ApJ, 456, 902
Saio, H. 1981, ApJ, 244, 299
Stankov, A., & Handler, G. 2005, ApJS, 158, 193
Sterken, C., Jerzykiewicz, M., & Manfroid, J. 1986, A&A, 169, 166
Walker, G., et al. 2003, PASP, 115, 1023
Yoshida, S., & Eriguchi, Y. 2001, MNRAS, 322, 389